Original Research

Revista Brasileiro de Física Médica (2026) 20: 871

Porosity Analysis of Bones by Double-Beam Acoustography

Dorival Mantovani[1], Frederico possato Tagliaferro[1], João Henrique Uliana [1],Reinaldo Cesar[2], Theo Zeferino Pavan[1], Antonio Adilton Oliveira Carneiro[1]

[1]Department of Physics, Faculty of Philosophy, Sciences and Letters of Ribeirão Preto, University of São Paulo, Ribeirão Preto, Brazil.
[2]Faculty of Electrical and Computer Engineering, University of Campinas (Unicamp), Campinas.

Abstract

Dual-beam acustography is an elastography technique that uses focused ultrasonic radiation to extract mechanical information through spectral analysis of the acoustic signal generated by the interaction of the ultrasonic pulse with the medium's structure. This study focuses on applying dual-beam acustography to analyze the porosity of human bone. The project involves measuring and analyzing trabecular bone samples from human vertebrae, with ethical approval. These samples, previously tested for mechanical properties at the Laboratory of Manufacturing and Precision Engineering at the School of Engineering of São Carlos, were prepared using a 3D-printed support and analyzed in a water tank with an ultrasonic transducer and hydrophone. Additionally, photoacoustic microscopy was incorporated to provide a complementary perspective, enhancing the understanding of bone porosity. The comparison between techniques revealed similar signals for assessing bone porosity. The acoustic signal showed a moderately strong correlation with the bone quality index (BQI) and a moderate correlation with the elastic modulus (E), suggesting that samples with higher BQI and E exhibit higher signal levels. The tensile stress at the fracture resistance limit (TLRF) showed a strong correlation with the signal, whereas the strain at the fracture resistance limit (DLRF) exhibited a weak correlation with the signal. These results indicate that TLRF is a good indicator of bone integrity, while DLRF may not be suitable for general assessments.

Keywords*: double-beam acoustography; trabecular bones; photoacoustic microscopy.*

1. Introduction

1.1. Contextualization

Trabecular bone tissue is characterized by a spongy and highly porous structure (1) found at the ends of long bones and in central regions such as the vertebrae. This structure consists of a complex network of interconnected columns and layers, known as trabeculae (2), with an average thickness of approximately 50 μm (3). Characterizing the material properties of trabecular tissue is of great importance for understanding its elastic and failure behaviors. Such understanding is essential for medical applications, including prosthesis development, orthopedic surgery planning, and fracture risk assessment, particularly in patients with osteoporosis (4).

Although techniques such as dual-energy X-ray absorptiometry (DEXA) and micro-computed tomography (micro-CT) are considered gold standards for bone structural analysis, their reliance on ionizing radiation limits their applicability for repeated in vivo assessments. While this limitation is not critical for ex vivo studies, it becomes relevant in clinical scenarios, where patient safety and dose accumulation must be considered. In this context, non-ionizing techniques such as dual-beam acoustography and photoacoustic microscopy emerge as promising alternatives. Beyond avoiding ionizing radiation, these techniques enable the assessment of mechanical-related properties by analyzing the intensity and spectral characteristics of the acoustic signals generated by the interaction between ultrasonic excitation and the bone microstructure, which are associated with bone strength and integrity (5). Therefore, the present ex vivo study aims to validate the technique under controlled conditions as a step toward its future application in clinical and in vivo environments.

1.2. Dual-Beam Acoustography

Dual-beam acoustography employs two simultaneously focused ultrasonic waves at the same point, with a slight frequency difference between them, typically in the kilohertz range. This setup results in the generation of an acoustic response at a frequency equal to the difference between the frequencies of the two incident waves. In this method, the higher-frequency waves interact with the tissue, triggering a response at a lower frequency that carries mechanical information specific to the tissue region where the beams intersect.

This acoustic response is not directly proportional to the ultrasound beam (6), meaning that the behavior of biological tissue in response to ultrasound does not follow a simple linear relationship, as observed in acoustic and biomedical ultrasound models. Nonlinear interactions can lead to phenomena such as harmonic generation, amplitude modulation, and frequency shifts (7). These effects can be exploited to extract additional information about the tissue's mechanical and structural properties, such as porosity. For this purpose, the signal-to-noise ratio (SNR) is adopted as a metric, as it quantifies the detectability of the nonlinear difference-frequency response while minimizing the influence of experimental and instrumental sources of variability.

In trabecular bone, increased porosity is generally associated with decreased bone mineral density and greater fracture susceptibility. Thus, reduced density and tissue integrity may be reflected in lower SNR values in dual-beam acoustography.

1.3. Photoacoustic Microscopy

Photoacoustic microscopy is an imaging technique based on the photoacoustic effect. This phenomenon occurs when a sample absorbs light, resulting in a slight local temperature increase, which in turn generates a pressure rise due to thermoelastic expansion (8,9). This pressure increase, influenced by the light intensity and the material's optical, thermal, and mechanical properties, gives rise to a pressure wave known as a photoacoustic wave. The photoacoustic wave is detected by an ultrasonic transducer and converted into an electrical signal. This signal is then amplified, digitized, and transferred to a computer for further analysis.

1.4. Objective

The main objective of this study was to characterize human trabecular bone samples in terms of porosity and microstructure-related mechanical response using the dual-beam acoustography technique. In addition, a subset of the same samples was analyzed by photoacoustic microscopy with respect to the same parameters. The results obtained from both techniques were compared with each other, as well as with previously measured mechanical parameters, in order to evaluate the consistency and complementarity of the two methods in the characterization of trabecular bone quality. Both methods were employed to assess variations in the acoustic response of the samples, quantified by means of the SNR.

2. Materials and Methods

2.1. Samples and Mounting

The human trabecular bone samples were acquired and approved under Research Protocol No. 408/11 by the Research Ethics Committee of the School of Medicine of the University of São Paulo. The samples are cylindrical in shape, approximately 2 cm in height and 1 cm in diameter (Figure 1). Due to their size and the need to obtain images with minimal noise, a circular holder was designed and 3D printed to accommodate the samples during scanning, as shown in Figure 1.

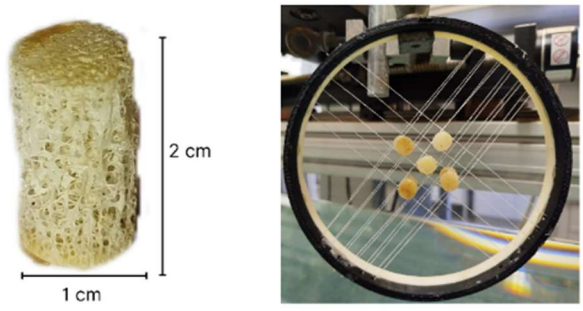

Figure 1. Left: Image of one of the trabecular bone samples used in the experiment. Right: Circular holder 3D printed. Holes were made in the structure so that cotton threads could hold the samples in place. Source: The author.

Using a circular holder with cotton threads proved preferable to placement in a gelatinous paraffin base (Figure 2), since movement of the support during sample scanning causes vibrations in the material, resulting in unwanted signals detected by the hydrophone.

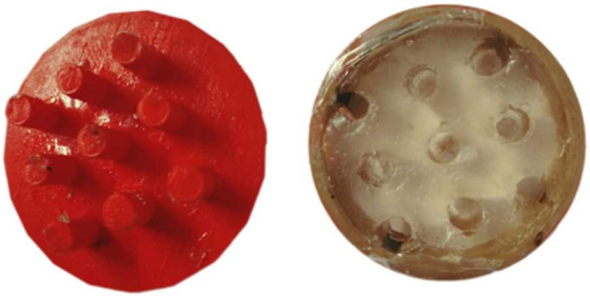

Figure 2. Left: Mold of the 3D-printed holder. Right: Gelatinous support for sample accommodation. Source: The author.

2.2. Dual-Beam Acoustography

The acoustography system setup is shown in Figure 3. In a water tank measuring 40 x 52 x 100 cm³, a confocal piezoelectric ceramic transducer operating at 3 MHz and an ITC-6050C hydrophone, pre-amplified with an acquisition bandwidth of 2-80 kHz, were positioned. Both remained immersed in water during the experiment. In addition, above the tank, a three-axis positioning system was connected to the control hardware (National Instruments PCI-7340 and National Instruments UMI-7774), enabling sample movement for scanning.

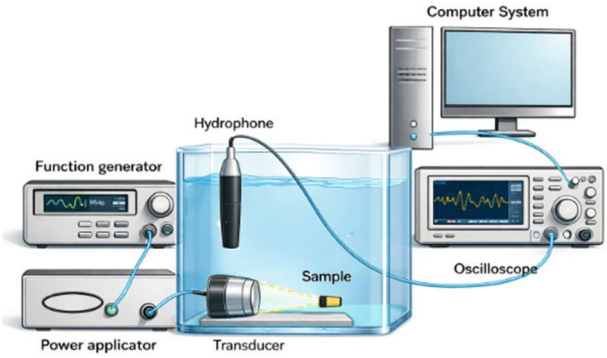

Figure 3. Diagram of the dual-beam acoustography experimental system. Source: The author.

The ultrasound transducer is responsible for ultrasonically exciting the sample, generating focused ultrasonic beams directed at the target. It was connected to a 20 dB gain amplifier operating in two independent channels. The excitation signals were controlled by two function generators: the Agilent 33622A (dual-channel) for adjusting the frequency, pulse length, and amplitude of the acoustic beams; and the Agilent 33220A (single-channel) for controlling the pulse trigger synchronized with the acoustography signal acquisition.

Acoustic signals were acquired using the hydrophone connected to a National Instruments PCI-5122 oscilloscope board. A common metric for evaluating signal quality in acoustography is the signal-to-noise ratio, calculated according to Equation 1:

$$SNR = 20.log_{10}\left(\frac{Mean\ Signal}{Noise\ Standard\ Deviation}\right) \quad (1)$$

The use of SNR instead of the average signal alone ensured better image quality, since the absolute intensity could vary with electronic gain, laser energy per pulse, and transducer alignment. Furthermore, tank vibrations, misalignments, reflections, and laser pulse instabilities generate background fluctuations, so that the SNR quantifies how much the signal stands out from these fluctuations. Higher SNR values indicate better signal quality and more reliable measurements of the sample's mechanical response.

For evaluating sample positioning relative to the ceramic transducer and hydrophone, a pulse-receiver device (Olympus Panametrics-NDT 5800) connected to an Agilent MSO7104B oscilloscope was used. All positioning, scanning, and signal acquisition parameters were controlled via software developed in LabVIEW (NI LabVIEW 2016, National Instruments).

Scanning was performed with the trabecular bones immersed in water. Due to the high porosity of the samples, to avoid trapped air bubbles, the samples were placed in a vacuum chamber under negative pressure and then submerged in water. Another approach involved submerging the samples several hours before the experiment and using a pipette to eject water, allowing bubbles to rise from the trabeculae to the surface over time.

2.3. Photoacoustic Microscopy

The experimental photoacoustic microscopy system is shown in Figure 4. An Nd:YAG LASER (Brio, Quantel, France) emits short light pulses. The Q-switch delay was set to 400 microseconds to optimize experimental conditions, ensuring that the laser pulse is released at the ideal time for data acquisition. The light passes through a beam splitter, and the higher-energy beam is collimated and redirected using a right-angle prism. Then, the beam is focused by a biconvex spherical lens with a 20 cm focal length. The entire system was aligned to ensure beam integrity. The sample, immersed in water, was held in place by a clamping holder connected to a three-axis stage for scanning.

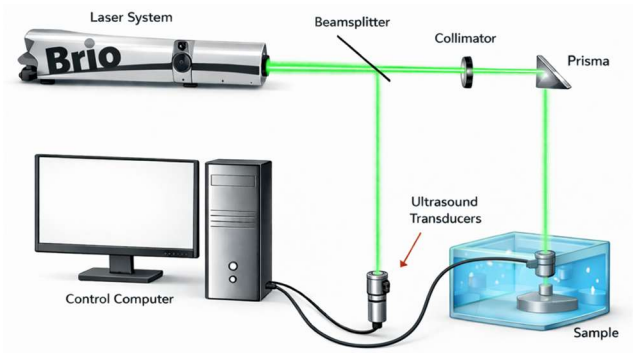

Figure 4. Schematic representation of the experimental setup for photoacoustic microscopy. Source: The author.

Due to thermoelastic expansion triggered by laser excitation of the sample, photoacoustic waves are generated. These waves are detected by a hollow ultrasonic transducer positioned above the sample. The transducer converts the sound waves into electrical signals that can then be processed and interpreted. All acoustic experiments were conducted in the laboratories of the Medical Instrumentation and Ultrasound Innovation Group (GIIMUS) of the Department of Physics at the School of Philosophy, Sciences, and Letters of Ribeirão Preto.

3. Results and Discussion

From the data obtained through dual-beam acoustography, image processing was performed using MATLAB software (R2020a). A region of interest was manually selected three times in the heatmap of each sample. Subsequently, the SNR ratio was calculated using Equation 1 for nine trabecular bone samples, as shown in Table 1.

Table 1. SNR values and their uncertainties for the trabecular bone samples obtained through dual-beam acoustography.

Sample T12	SNR (a.u.)	σ SNR (a.u.)
2003	7.16	0.24
2188	6.92	0.29
2425	6.98	0.39
2432	6.39	0.09
2434	6.67	0.38
2454	6.39	0.04
2194	6.37	0.24
2421	6.43	0.30
2867	6.12	0.59

Source: The author (2026).

The results obtained were compared with previously acquired values of the elastic modulus (E), bone quality index (BQI), tensile limit of fracture resistance (TLRF), and strain at the deformation at the fracture resistance (DLRF) for each bone, as shown in Table 2 below.

Table 2. Values of elastic modulus, BQI, TLRF, and DLRF for each analyzed sample group.

Group	T12	BQI (a.u.)	E (MPa)	TLRF (MPa)	DLRF (a.u.)
NORMAL	2003	130,67	109,25	2,94	5,26
NORMAL	2188	125,83	144,77	2,02	2,90
NORMAL	2425	98,83	120,28	1,42	2,69
OSTEOPENIC	2432	78,83	46,08	0,77	3,24
OSTEOPENIC	*2434*	80,33	84,28	1,48	3,35
OSTEOPENIC	2454	75,50	64,55	0,68	2,49
OSTEOPOROTIC	2194	56,17	47,43	0,52	2,34
OSTEOPOROTIC	2421	52,50	20,08	0,28	3,04
OSTEOPOROTIC	2867	55,83	38,21	0,61	3,46

Source: The author (2026).

The mechanical parameters reported in Table 2 were obtained in a previous study using the same intact bone samples employed in the present work. The BQI was determined by quantitative ultrasound, whereas the elastic modulus, TLRF, and DLRF were measured through compression tests, with the cross-sectional area determined using a caliper. These reference data are used here for comparison with the acoustic measurements.

A plot was then constructed to illustrate the relationship between the signal and the elastic

modulus for each sample, followed by a linear regression, as shown in Figure 5.

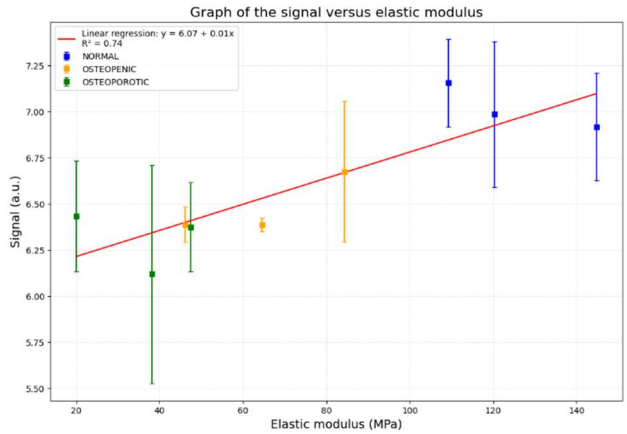

Figure 5. Plot of the signal-to-noise ratio versus the elastic modulus of the analyzed samples. Source: The author.

According to the graph, there is a correlation between the signal and the elastic modulus in the analyzed samples, indicating a trend where samples with a higher elastic modulus exhibit stronger signals. This relationship was expected, as the elastic modulus of bone is influenced by bone mineral density (BMD), microarchitecture, and material quality, including factors such as collagen content and fiber organization (10). Therefore, the measured signal is directly affected by the elastic modulus. However, other factors, such as tissue heterogeneity or distinct structural characteristics, also influence this relationship, justifying the moderate correlation observed in the graph.

Additionally, it was observed that the osteoporotic group showed lower elastic modulus values compared to the normal group. This finding aligns with the scientific literature, which shows that osteoporosis, a condition characterized by reduced BMD and deterioration of bone microarchitecture, results in a significant decrease in trabecular bone stiffness (as indicated by the elastic modulus).

Since the elastic modulus is highly dependent on bone density, which is inversely related to porosity, increased porosity leads to reduced bone density, and consequently, a lower elastic modulus. Porosity affects the connectivity and thickness of the trabeculae (the small rods or plates forming the internal structure of bone). As porosity increases, there is less solid material to resist deformation, reducing overall bone stiffness. Thus, osteoporotic bone samples are expected to exhibit lower elastic modulus values compared to normal bone samples.

Another parameter related to porosity is the tensile limit of fracture resistance. TLRF is the maximum stress the bone can withstand before fracturing. This property is extremely sensitive to the microarchitecture of trabecular bone, including its porosity. Therefore, a diagram illustrating the relationship between signal and TLRF was constructed, as shown in Figure 6.

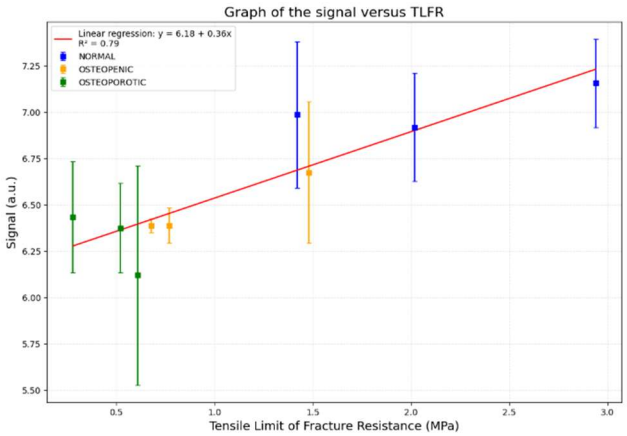

Figure 6. Representation of the signal-to-noise ratio versus the tensile stress at the fracture resistance limit. The red line represents the linear regression of the data. Source: The author

Similarly, the TLRF curve revealed a significant linear relationship with the signal, with a coefficient of determination of 0.79. This suggests that the trabecular bone's ability to withstand stress up to the fracture point is directly related to the measured signal. As TLRF is also negatively affected by porosity, increased porosity reduces bone resistance to fracture. This behavior is due to the higher porosity, which creates stress-concentration sites and reduces the number of interconnected trabeculae, thereby weakening the bone and making it more susceptible to fractures. Thus, TLRF is highly dependent on structural integrity and bone microarchitecture, which are compromised in high-porosity states.

The strain at the deformation at the fracture resistance was also analyzed. A chart depicting this relationship is shown in Figure 7.

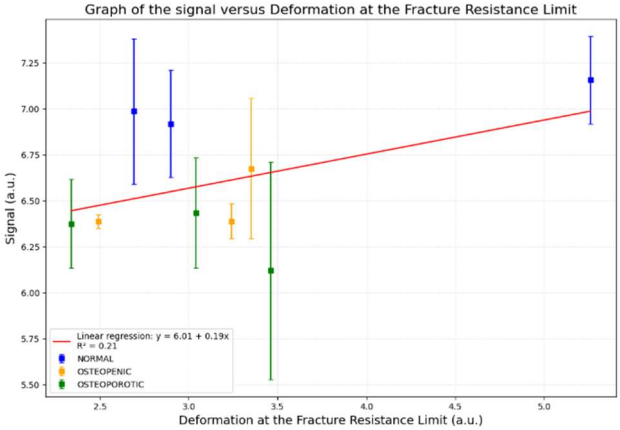

Figure 7. Graph of the signal-to-noise ratio versus deformation at the fracture resistance limit. Source: The author

According to the graph, there was a weak correlation between these two variables for the analyzed trabecular bone samples. Only 21% of the signal variability can be explained by the DLRF, meaning that most of the variation observed in the signal is not directly related to DLRF.

This relationship can be explained by considering the biomechanical and microstructural characteristics of trabecular bone. DLRF represents the maximum strain the bone can undergo before fracturing. Unlike the elastic modulus or TLRF, which are directly

influenced by stiffness and structural strength, DLRF is more associated with the bone's deformability before collapse. Trabecular bone is inherently heterogeneous and anisotropic, composed of irregularly organized trabeculae, which can lead to significant variability in deformation response under load. Moreover, DLRF may be less dependent on mineral density and overall stiffness, and more influenced by local factors such as trabecular orientation and microarchitectural connectivity. This implies that DLRF may not be a good predictor of global bone integrity measures, such as the analyzed signal.

The Figure 8 shows the linear relationship between the signal and the BQI.

The coefficient of determination of 0.80 indicates a moderately strong association. This suggests that bones with higher BQI tend to produce more intense acoustic signals. The sample distribution reveals that osteoporotic bones, with lower BQI, generate lower signals, while normal bones, with higher BQI, produce higher signals. Osteopenic bones occupy an intermediate position, both in terms of BQI and signal intensity. Moreover, the data also indicate that signal variability within each group is more pronounced at the extremes (normal and osteoporotic), suggesting that even within the same clinical group, there may be significant structural differences among samples.

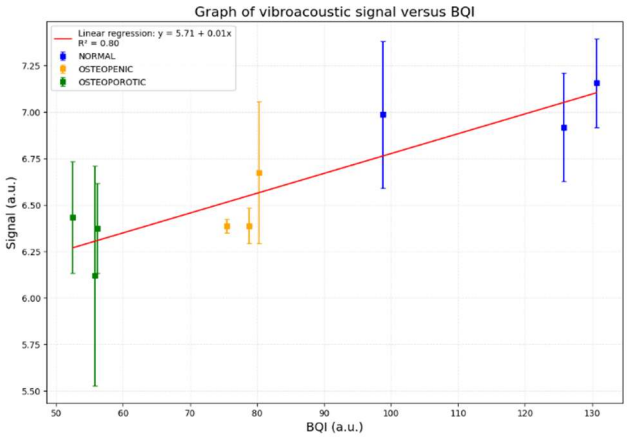

Figure 8. Graph of the signal-to-noise ratio versus BQI. Source: The author

Thus, the positive slope of the regression line confirms a progressive increase in signal as BQI increases. This behavior supports the hypothesis that bones with better structural integrity (higher density and lower porosity) respond more efficiently to ultrasonic excitation, generating stronger and higher-quality signals.

To determine whether there is a relationship between the vibroacoustic and photoacoustic signals, the SNR was analyzed for three bone samples, as shown in Figure 9.

The similarity in signal levels suggests that both vibroacoustic and photoacoustic techniques, although based on different principles, are capturing similar characteristics of the bone samples, such as porosity. If the signals are comparable in magnitude, it may indicate that both methods are effective in assessing structural and mechanical properties of trabecular bone. This similarity can be interpreted as evidence that both techniques offer a comprehensive analysis of bone quality.

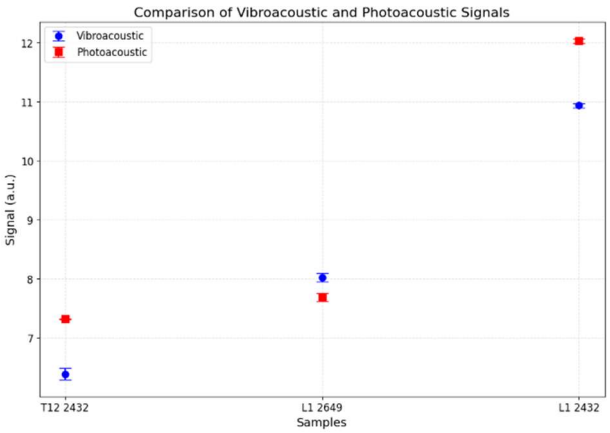

Figure 9. Plot of the vibroacoustic and photoacoustic signal measurements, with their respective uncertainties associated with each of the three samples. Source: The author

In Figures 10 and 11, the spatial distributions of the acoustic response for the same sample are shown, obtained using dual-beam acoustography and photoacoustic microscopy, respectively.

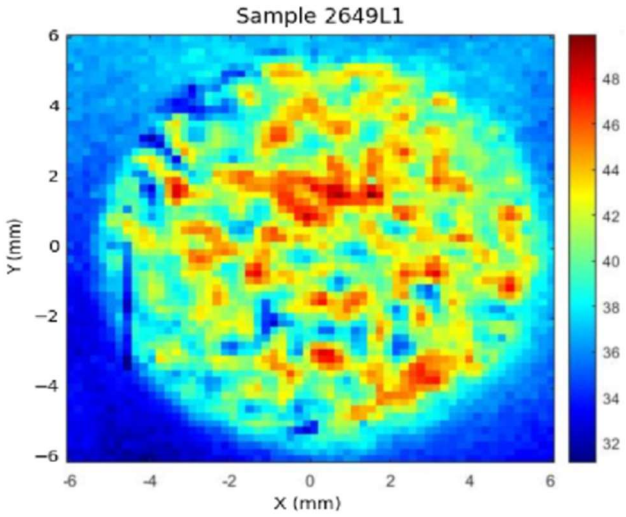

Figure 10. Spatial distribution of the acoustic response in the trabecular bone sample 2649L1 obtained using dual-beam acoustography. Regions of higher signal intensity are highlighted in the intensity map. Source: The author

In both images, regions of higher signal intensity are highlighted, indicating areas with stronger acoustic response. Despite this qualitative agreement, noticeable differences in the spatial localization and distribution of high-intensity regions can be observed between the two techniques. These discrepancies can be attributed to differences in the experimental configurations, signal generation mechanisms, and spatial resolution inherent to each method. Even with these disparities, both techniques exhibited comparable SNR, as shown in Figure 9. This result supports the use of SNR as a robust metric for comparison in this study, as it is less sensitive to positional mismatches and experimental variability.

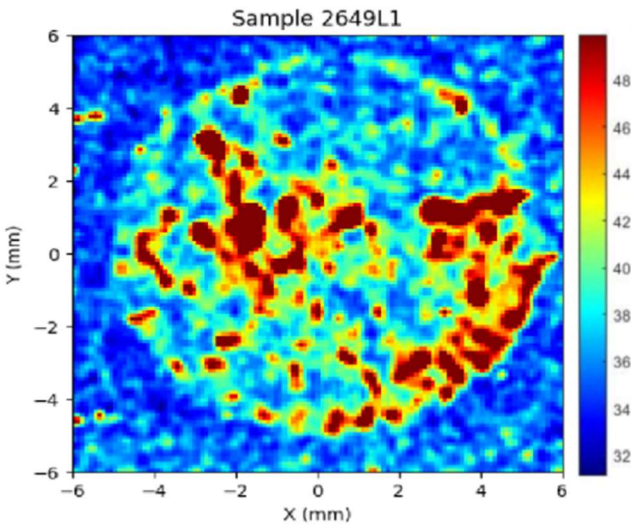

Figure 11. Photoacoustic microscopy image of trabecular bone sample 2649L1, showing the spatial distribution of the acoustic response and highlighting areas of higher signal intensity. Source: The author

Further experiments and analyses are required to investigate how the specific physical principles of each technique influence their sensitivity to bone microstructure and porosity, as well as to better understand the origin of the observed spatial differences.

5. Conclusion

The results indicated a correlation between the acoustic signal and the mechanical properties of trabecular bone. A relationship between the signal and the elastic modulus was observed, reflecting that samples with higher elastic modulus generally exhibited higher signal values. Consequently, the osteoporotic group showed lower elastic modulus values, corroborating the literature that describes reduced stiffness in osteoporotic bones due to increased porosity and loss of structural integrity. The tensile limit resistance to fracture showed a significant linear correlation with the signal. TLRF, which is strongly influenced by porosity, decreases as porosity increases due to the reduction in the number of interconnected trabeculae, which are crucial for the mechanical strength of bone. In contrast, the deformation at the fracture resistance limit showed a weak correlation with the signal ($R^2 = 0.21$), indicating that signal variability is not directly explained by the bone's ability to deform before fracture.

Additionally, the Bone Quality Index showed a moderately strong positive correlation with the acoustic signal ($R^2 = 0.80$), indicating that bones with greater structural integrity—characterized by higher density and lower porosity—tend to produce more intense signals. This association reinforces the hypothesis that the acoustic response is sensitive to variations in bone microarchitecture. Notably, osteoporotic samples exhibited lower BQI and signal values, while normal bones showed higher values for both parameters, with osteopenic samples occupying an intermediate position. The variability of the signal within each clinical group, particularly at the extremes, suggests internal heterogeneity even among samples of similar classification.

Finally, the comparison between vibroacoustic and photoacoustic signals revealed similar values, suggesting that both techniques are capable of capturing similar characteristics of trabecular bone, such as porosity.

Acknowledgments

Partial financial support was provided by the FAPESP grants 23/13435-7, 18/16939-8, and 22/07463-5, CNPq grant 311224/2021-0, and CAPES – Funding Code 001.

References

1. Jee WSS. Bone histomorphometry: techniques and interpretations. Boca Raton: CRC Press; 2001.
2. Lucchinetti E, Thomann D, Danuser G. Micromechanical testing of bone trabeculae - potentials and limitations. J Mater Sci. 2000;35:6057–65. https://doi.org/10.1023/A:1026748913553
3. Lips P, Courpron P, Meunier PJ. Mean wall thickness of trabecular bone packets in the human iliac crest: changes with age. Calcif Tissue Res. 1978;26(1):13–7.
4. Oftadeh R, Perez-Viloria M, Villa-Camacho JC, Vaziri A, Nazarian A. Biomechanics and mechanobiology of trabecular bone: a review. J Biomech Eng. 2015;137(1):0108021–15. doi: 10.1115/1.4029176.
5. Cai X, Zhang YS, Xia Y, Wang LV. Photoacoustic microscopy in tissue engineering. Mater Today. 2013;16(3):67–77. https://doi.org/10.1016/j.mattod.2013.03.007
6. Silva GT, Mitri FG. Difference-frequency generation in vibro-acoustography. Phys Med Biol. 2011;56(18):5985–93. Available from: https://iopscience.iop.org/article/10.1088/0031-9155/56/18/013/pdf
7. Braz GA. Implementação de uma técnica de caracterização de tecidos biológicos baseada na emissão acústica em baixa frequência (kHz) de alvos excitados em alta frequência (MHz) [dissertação]. São Paulo: Universidade de São Paulo; 2020. Available from: https://www.teses.usp.br/teses/disponiveis/59/59135/tde-31072020-162346/publico/Corrigida_GuilhermedeAraujoBraz.pdf
8. Uliana JH, Miano ACC, Silva GT, Mitri FG, Baffa O. Photoacoustic microscopy of sandstone reservoirs rocks. In: 2023 IEEE International Ultrasonics Symposium (IUS); 2023 Sep; Montreal, Canada. Piscataway: IEEE; 2023. https://doi.org/10.1109/IUS51837.2023.10308378
9. Uliana JH. Sistemas de imagem e espectroscopia fotoacústica [tese]. Ribeirão Preto: Universidade de São Paulo; 2021. Available from: https://www.teses.usp.br/teses/disponiveis/59/59135/tde-10102022-092326/
10. Keaveny TM, Morgan EF, Niebur GL, Yeh OC. Biomechanics of trabecular bone. Annu Rev Biomed Eng. 2001;3:307–33. doi: 10.1146/annurev.bioeng.3.1.307.
11. Cezar R. Caracterização de materiais por técnicas não destrutivas [tese]. São Carlos: Escola de Engenharia de São Carlos, Universidade de São Paulo; 2015. Available from: https://teses.usp.br/teses/disponiveis/18/18150/tde-09022015-113119/publico/Tese_doutorado_Reinaldo_Cesar.pdf

Contact:

Dorival Mantovani
University of São Paulo
Department of Physics, Faculty of Philosophy, Sciences and Letters of Ribeirão Preto, USP, Vila Monte Alegre, Ribeirão Preto, São Paulo, 14040-900, Brazil
dorival.mantovani@hotmail.com